Journal of
Ceramic Science
and Technology

J. Ceram. Sci. Technol. 1-10 (2021)
DOI: 10.4416/JCST2020-00022
available online at: http://www.ceramic-science.com

The Effect of the P/Si Ratio on the Preparation and Properties of Phosphoric Acid-Metakaolin Geopolymers

E. Furlani*[1], E. Aneggi[1], A. Rondinella[1], M. Zanocco[2], L. Fedrizzi[1], S. Maschio[1]

[1]University of Udine, Polytechnic Department of
Engineering and Architecture, Via Del Cotonificio 108, 33100 Udine, Italy
[2]Ceramic Physics Laboratory, Kyoto Institute of
Technology, Sakyo-ku, Matsugasaki, 606 – 8585 Kyoto, Japan
received September 29, 2020; received in revised form February 26, 2021; accepted February 27, 2021

Abstract

The present research deals with the production and characterization of geopolymers prepared by mixing metakaolin, different amounts of phosphoric acid solution and water. Hardening was performed by aging the geopolymeric pastes in a climatic chamber.

The workability of the pastes has been improved while the H_2O/total solid content has been kept constant and the P/Si ratio increased. However, such a benefit implies considerable heat output, which must be controlled in order to limit the formation of extended fractures. The compressive strength of the hardened materials increases with increasing P/Si ratio at a constant H_2O/total solid content, whereas their strength decreases with increasing H_2O/total solid content at a constant P/Si ratio. The open macroporosity, which is directly dependent on the total amount of water added to the geopolymeric pastes, may explain the above results better than the nano/microporosity and/or chemical bonds that contribute to building up the materials' textural features.

Keywords: Geopolymers, phosphoric acid, workability, FTIR, pore size distribution

I. Introduction

Geopolymers are ceramic materials prepared from starting powders that can be consolidated with a chemical method instead of with a traditional sintering process. They may be synthesized by means of alkaline or acid treatment; the former route is documented extensively in the literature [1–8], the latter is a more recent and less documented preparation process [9–13].

Today, the possibility of using alkali-activated alumino-silicate powders as a hydraulic binder that could replace Ordinary Portland Cement (OPC) in the manufacturing of engineering structures is generally accepted [14–17]; at the same time it is also known that such geopolymers could limit the release of many hazardous compounds from inorganic waste or polluted products [18–21] or be used to inertize some industrial by-products [22–26].

The reaction that leads to the geopolymeric structure, however, occurs not only with the addition of an alkaline activator, but also after the alumino-silicate source is mixed with a solution of phosphoric acid and water. This class of geopolymers, formerly well known in the field of refractory materials, has been recently rediscovered as it has been demonstrated that it could develop fair thermal [13,27–28], mechanical [29–30] or electric [31–33] properties provided that the P/Si (P/Al) ratio is confined within appropriate ranges. In addition, their production does not require the use of caustic reagents and they behave better in acid environments.

In particular, Celerier *et al.* [34] showed that the behaviour of geopolymers depends on the metakaolin starting powder used for their production; they reported that the Si-Al-P ternary diagram can be divided into distinct zones, which permit to obtain geopolymers that exhibit different behaviour during consolidation so that the hardened materials may then have different fire or water resistance. On the other hand, Louati *et al.* [29] prepared several geopolymers starting from phosphoric acid and illito-kaolinitic clay; they reported that the maximum compressive strength is achieved when the composition of the starting components corresponds to a Si/P ratio of 2.75. Higher or lower ratios lead to lower strength values.

Following on from the above-cited papers, in the present research several geopolymers have been prepared with increasing P/Si ratio (four in total) and the properties of the resulting hardened samples have been measured. The first composition was selected with the same P/Si ratio as the one that developed the maximum strength according to the paper by Louati *et al.* [29], as a particular type of reference composition. This was used as the one with the minimum P/Si ratio. For each investigated P/Si ratio, the minimum and maximum amount of additional water (in excess of the amount added with the H_3PO_4 solution) was determined with the slump flow test, reported as the water/total

* Corresponding author: erika.furlani@uniud.it

solid content ratio and discussed in terms of paste workability. This approach enabled the identification of materials prepared from pastes with different P/Si ratios, but the same H_2O/total solid content, permitting a comparison between their characteristics.

Aim of the present research is to find out how the P/Si ratio affects the minimum amount of water required for paste workability as well as the properties of the hardened materials. Geopolymeric hardened samples were then characterized by means of XRD and FTIR spectroscopy analysis, compressive strength, water absorption, pore size distribution, specific surface area, SEM investigation and stability in water.

II. Experimental

(1) Starting materials

Starting materials for the geopolymers synthesis were Argical M1200 calcined kaolin (metakaolin-MK) supplied by Imerys Refractory Minerals and a commercial phosphoric acid solution (85 wt%) supplied by Titolchimica (Pontecchio Polesine, Rovigo, Italy). The chemical composition of metakaolin was analysed with a Spectro Mass 2000 Induced Coupled Plasma (ICP) mass spectrometer and is reported in Table 1 together with the loss on ignition (LOI), which was determined after thermal treatment at 1 000 °C for 2 h. The specific gravity, measured in compliance with the ASTM C127 and C128 standards, is 2.59 g/cm^3.

(2) Preparation and characterization of the starting materials

The mix proportion design is reported in Table 2, which also shows the sample identification codes (used hereafter), P/Si ratio, slump flow, water absorption and compressive strength for all compositions. The P/Si was built up based on the assumptions that only 90 wt% of MK reacts for geopolymerization [35,36] and the water/total solid content ratio also takes into account the water contained in the phosphoric solution.

The particle size distribution (PSD) of the as-received MK was determined with a Horiba LA950 laser scattering particle size analyzer. Analyses were performed in water after 3 min sonication. PSD curves (cumulative representation) are displayed in this work with logarithmic abscissa.

Crystalline phases of the MK as well as those of the hardened geopolymers were investigated by means of X-ray diffraction (XRD). The XRD patterns were acquired with a Philips X'Pert diffractometer operating at 40 kV and 40 mA and using a Ni-filtered Cu-Kα radiation beam. Spectra were collected using a step size of 0.02° with a counting time of 40 sec per angular abscissa in the range of 10 – 80°. The Philips X'Pert HighScore software was used for phase identification whereas their semi-quantitative evaluation was obtained in accordance with the RIR method [37].

Table 1: Chemical composition (reported in terms of oxides) and LOI of the Argical M1200.

	SiO_2	Al_2O_3	K_2O+Na_2O	Fe_2O_3	TiO_2	CaO+MgO	Others	LOI
wt%	55	39	1.3	1.1	1.5	0.7	1.4	1

Table 2: Mix proportion design of the compositions prepared. The table also displays P/Si ratio, slump flow, water absorption and compressive strength of all compositions.

Composition symbolic name	MK (g)	H_3PO_4 (g)*	H_2O (cm^3)	H_2O/total solid content	P/Si	Slump flow (cm)	Ass H_2O (%)	σ (MPa)
PG1	100	33.6	68.3	0.57	0.36	18.5	40	8
PG2	100	33.6	61.8	0.52	0.36	14.5	36	14
PG3	100	33.6	55.4	0.47	0.36	11.4	30	17
PG4	100	53.5	75.3	0.57	0.57	18	36	15
PG5	100	53.5	68.0	0.52	0.57	17	32	17
PG6	100	53.5	60.2	0.47	0.57	14.5	30	19
PG7	100	80.2	75.5	0.52	0.86	16.8	28	22
PG8	100	80.2	67.0	0.47	0.86	15.1	25	27
PG9	100	80.2	58.6	0.42	0.86	13.6	21	30
PG10	100	98.8	71.3	0.47	1.05	16.8	20	31
PG11	100	98.8	62.1	0.42	1.05	14.8	17	34

* Solution 85 wt%

(3) Sample preparation

Geopolymer samples were prepared according to the mixing proportions reported in Table 2 by mechanically mixing MK and phosphoric acid solution in different proportions. Mechanical mixing was performed in a Hobart stirrer (5 L capacity).

It has been observed that, during the first stage of homogenization, the slurries display high viscosity, which progressively decreases on further mixing, reaching a creamy consistency after about 5 min; mixing was successively prolonged for a further 15 min. At the end of the mixing process, the pastes were poured under vibration into high-density cylindrical nylon moulds, further vibrated for 2 min to remove air and sealed with a plastic film.

The spread-flow test was performed in order to evaluate the workability of the slurries [38,39]. In the present research, the slurries were poured into a truncated conical mould (top diameter = 70 mm, bottom diameter = 100 mm, height = 60 mm), which was filled up to the top; after 1 min, the conical mould was lifted vertically and the diameter of the cake after spreading was measured along two perpendicular directions. The mean value of the above two measurements was used to evaluate paste workability. The workability limit was assumed when the pastes did not expand after the mould had been lifted.

After moulding, hardening was performed by aging the geopolymeric pastes in a climatic chamber at 10 °C and 50 % relative humidity for 48 h followed by thermal treatment at 40 °C for ten days.

(4) Characterization of hardened materials

ATR-FTIR analysis was performed by means of a Nicolet iS™ 50 FTIR Fourier transform spectrometer using the attenuated total reflection (ATR) method. The IR spectra were recorded over a range of 500 – 4 000 cm^{-1} at a resolution of 2 cm^{-1} with 100 scans.

A spectrometer (Axis Ultra, Kratos, Manchester, UK) was used to perform X-ray photoelectron spectroscopy (XPS). An Al-kα monochromatic X-ray source was used. Low-resolution with wide-range scans were performed using 160 eV pass energy for 0.1 at% resolution. High-resolution scans were performed using a lower pass energy, 40 eV, thus improving the compositional resolution to 0.01 at%. The dimensions of the investigated areas were 700 µm x 300 µm, in order to obtain an average from the heterogeneities at each sample's surface. Commercially available software (CasaXPS, Casa Software Ltd., UK) was used to process the data. Argon sputtering was performed on all samples prior to the analysis, in order to remove adsorbed surface contaminants, using 4.2 keV beam energy, a gun angle of 45°, sample current of about 2 µA and raster area of 3 mm x 3 mm.

Compression tests were performed on cylindrical specimens with 60 mm diameter and 120 mm height (in accordance with the ASTM C39 standard), using an 810 Material Test System (MTS) with a crosshead speed of 2 mm/min. The data were averaged over three measurements for each composition.

A modified ASTM C 642 standard was followed to measure the water absorption of the hardened samples. The samples were placed in an oven at 80 °C ± 5 K for 24 h and weighed in air (W_1). They were successively aged in an autoclave at 120 °C and 2 kPa for 2 h using 2 L of water, cooled down to room temperature (in water), dried with a cloth and weighed again (W_2). Water absorption was evaluated according to the following equation:

$$W\ (\%) = 100\ (W_2\text{-}W_1)/W_1$$

Specific surface areas (A), pore size distribution and average pore size were determined on grit-like samples (dimensions approximately 2 – 3 mm) according to the B.E.T. method based on nitrogen adsorption at 77 K, using a Tristar 3000 gas adsorption analyser (Micromeritics).

The scanning electron microscope (SEM) investigation was performed by means of a Zeiss EVO40.

The materials' stability in water as well as their release were investigated with samples previously submitted to compressive strength tests: coarse particles were separated on a 9.5-mm sieve whereas pieces with diameters between 4 and 9.5 mm were used for a sort of leaching test adapted to this particular application. Coarse particles (size > 9.5 mm) were dried in an oven at 90 °C for 24 h and weighed; they were successively soaked in water for 24 h. After soaking, samples were dried and weighed again: the different weight, before and after the treatment, was used to determine the materials' stability in water. On the other hand, in order to investigate release, fifty grams of the samples (size 4 – 9.5 mm) were weighed into a 1000-ml polypropylene plastic bottle containing 1000 ml water. The suspensions were shaken for 18 h on an end-over-end shaker at a speed of 30 rpm and then filtered. The pH of the filtered solutions was measured with a Crison GLP21 pH-meter.

III. Results and Discussion

As can be seen in Table 1, the chemical analysis of the MK revealed the presence of high quantities of SiO_2, Al_2O_3 and minor amounts of other components in line with the nominal composition of this commercial product with a Si/Al atomic ratio of 1.19. The XRD analysis (Fig. 1) revealed the presence of muscovite (3 %) (PDF 00 – 046 – 0741), free quartz (4 wt%) (PDF 01 – 083 – 2465) and anatase (1 %) (PDF 01 – 071 – 1166) together with an amorphous phase highlighted by the presence of the amorphous hump emerging from the background line. Fig. 2 displays the PSD and cumulative curves of the MK powder, showing the presence of particles having a bimodal distribution highlighted by a small peak centred at around 300 nm and a larger one at around 7 µm.

The procedure followed for the preparation of all geopolymers (i.e. aging at low temperature inside a climatic chamber during the first stage of curing followed by thermal treatment) was established after several attempts, which showed a strong initial heat output being observed during the first hours after paste production [35,36], which is due to the rapid solubilization of the MK cryptocrystalline structure.

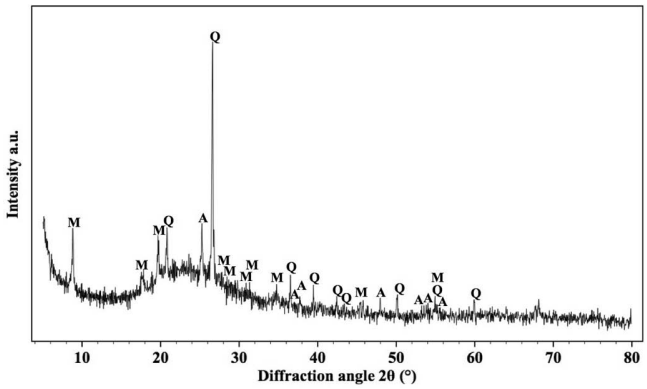

Fig. 1: X-ray diffraction pattern of the as-received metakaolin. Phases are identified with the following symbols: (M) = muscovite; (Q) = quartz; (A) = anatase.

Heating caused fast water evaporation followed by growth of extended cracks on the samples' surfaces and bulk. This statement is documented by a SEM investigation made on samples prepared without a controlled hardening process. Fig. 3 (a – d) show the free surface of the hardened samples PG3, PG6, PG8 and PG10 which have different P/Si ratio, but the same water to total solid content. It may be observed that, as the P/Si ratio is increased, porosity progressively decreases, whereas fractures look increased in number and/or dimension. Aging at 10 °C could appear excessive for compositions containing a low amount of phosphoric acid (namely those identified with symbols PG1 – PG6) which exhibit a relatively limited heat output, but proved necessary for compositions containing a high quantity of phosphoric acid (compositions PG7 – PG11) where the strong heat output, due to the high P/Si ratio, causes fast water evaporation, fast shrinkage and favours materials fracturing as has been clearly mentioned in the literature [40, 41]. The initial aging at low temperature allows control of the heat output after mixing and the preservation of the materials' integrity.

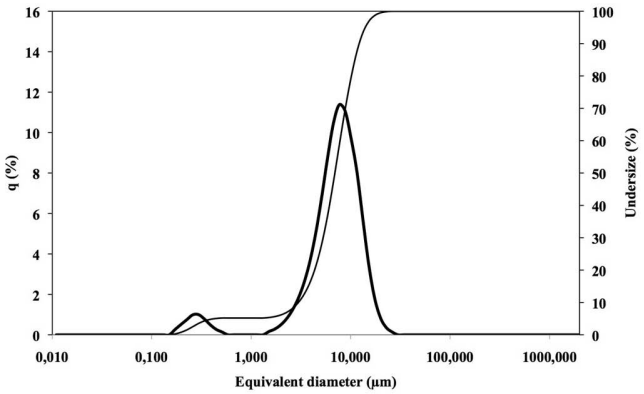

Fig. 2: Particle size distribution (left axis) and cumulative representation (right axis) curve of the as-received metakaolin.

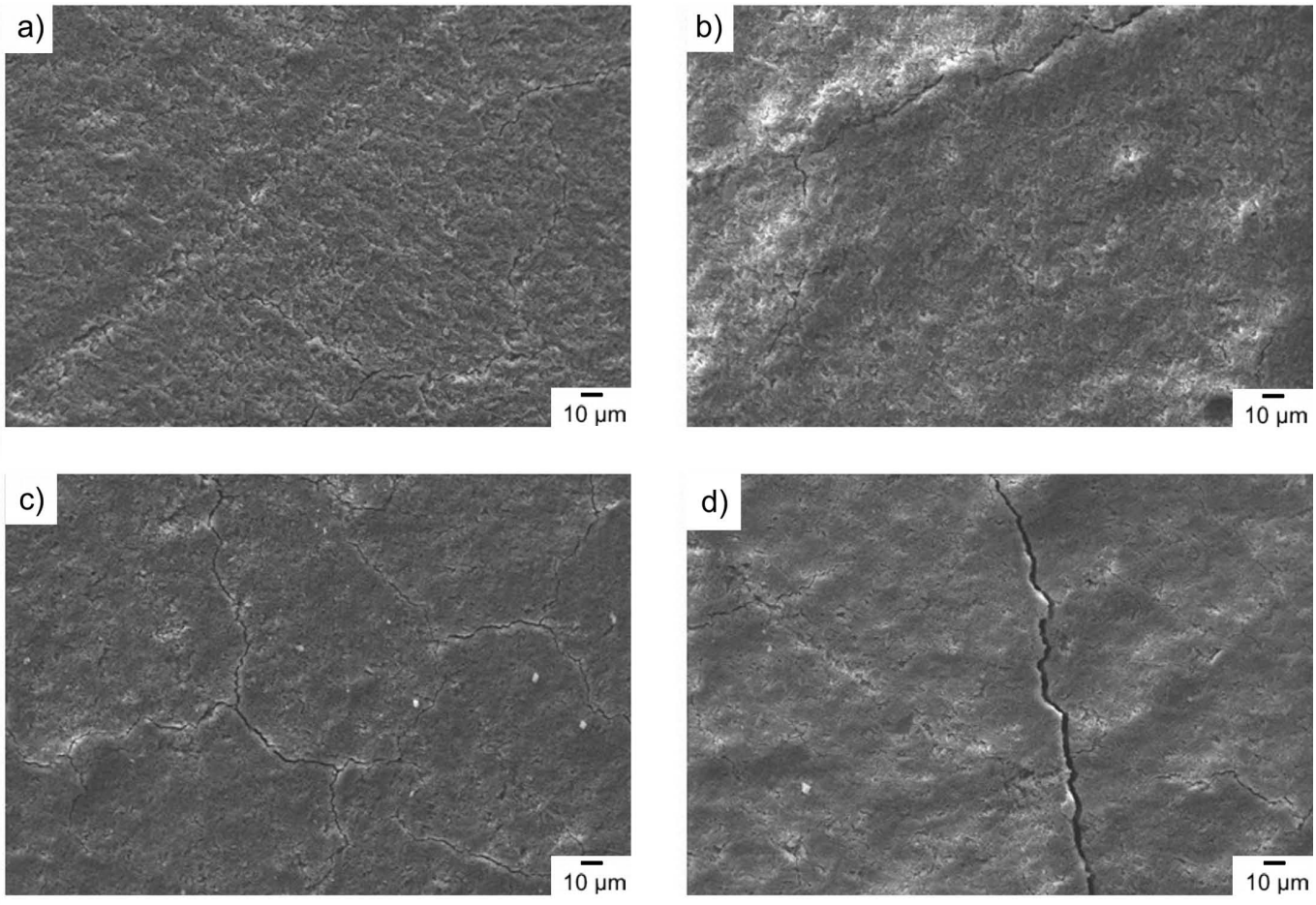

Fig. 3 a, b, c, d: SEM images of the free surface of samples PG3 (a), PG6 (b), PG8 (c) and PG10 (d) after uncontrolled consolidation.

Table 2 reports the average values of the slump (cm) for all the compositions whereas Fig. 4 shows the trend as a function of the P/Si ratio at constant water/total solid content (0.47). As expected, the slump values decrease, lowering the amount of water at a fixed P/Si ratio; on the other hand, it can be observed that, with an increase in the P/Si ratio, the workability of the pastes is improved for the same water/total solid content. In other words, by increasing the amount of phosphoric acid relative to the MK powder, the total amount of water might be reduced down to the workability limit, without precluding good homogenization of the starting components. For each P/Si ratio, the minimal slump value reported in Table 2 corresponds to the workability limit of the blends prepared using the 5-litre Hobart mixer. The workability limit of the compositions with the P/Si of 1.05 and 0.86 falls to the value of 0.42 of water/total solid content whereas that of the compositions with P/Si of 0.36 and 0.57 falls to the water/total solid content of 0.47. The authors are aware that, in case of a P/Si of 0.36, the lowest value of the water/total solid content leads to a paste that cannot be cast because of its plastic consistency. It seems reasonable that the workability test used in the present research is not applicable for that particular composition.

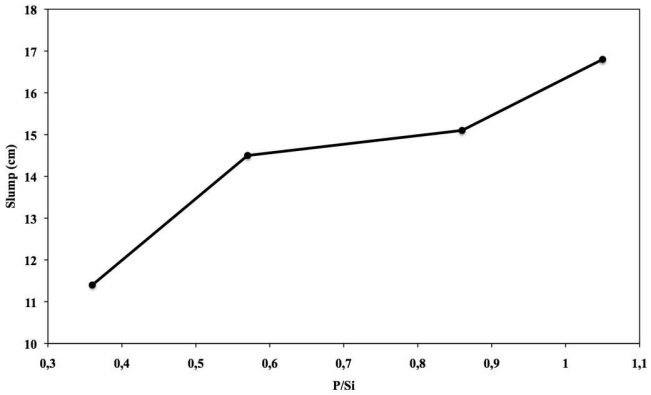

Fig. 4: Slump flow versus P/Si at a constant (0.47) H_2O/total solid content ratio.

The X-ray diffraction (Fig. 5) investigations performed on the hardened materials revealed that the crystalline quartz and anatase appear inert versus the phosphoric acid attack since they maintain similar intensity before and after geopolymerization [34] whereas the peaks of muscovite tend to decrease with an increasing amount of phosphoric acid added to the MK starting powder, thus revealing its moderate reactivity during the sol-gel reaction. In addition, it can be observed that the pattern collected on the MK shows a less intense amorphous hump, characteristic of the main reactive phase, located at approximately 25°± 0.5 which is also shifted towards higher degrees in hardened materials, thus showing that the cryptocrystalline structure of MK changes into a new one as an effect of the polymerization and appears to be independent of the P/Si ratio.

Fig. 6 compares ATR-FTIR spectra from metakaolinite (MK) and geopolymer (PG) samples. The green arrows in panel (a) highlight the absorption bands at about 1 646 and 3 290 cm^{-1}. They arise from the stretching and deformation modes of H-O-H and O-H in adsorbed water [42,43]. The bands at 546 cm^{-1} and 1 – 040 cm^{-1} in the MK spectrum (cf. the blue dotted lines in Figs. 6b and 6c) are attributed to Si-O-Si vibrations [43,44]. After geopolymerization, the spectral position of these bands shifts toward lower (cf. Fig. 6b) and higher (cf. Fig. 6c) wavenumbers, respectively. In the first case, a partial replacement of SiO_4 tetrahedra with PO_4 units can be hypothesized, resulting in a partial rearrangement of the local structure [42,43]; in the second one, a similar phenomenon could be due to a limited substitution of SiO_4 with AlO_4 groups [45]. The blue arrow in Fig. 6b identifies a peak at 785 cm^{-1} that can also be attributed to the Si-O-Si bonds [46] even if its intensity greatly decreases after the sol-gel reaction. The red arrow in Fig. 6b shows a band at 912 cm^{-1} representing P-O-Al bonds inside the samples [47]. This peak is absent in the MK spectra and appears only after reaction. From PG3 (P/Si ratio of 0.36) to PG10 (P/Si ratio of 1.05) the peak height gradually increases; its intensity is directly proportional to the amount of H_3PO_4 used as a reagent. The results from ATR-FTIR measurements suggest that Si-O-Si bonds are partially substituted by Si-O-P and Si-O-Al bonds [44,48], confirming XRD results and providing further insights into the structural and chemical changes occurring after geopolymerization. It follows that the main building block of phosphoric acid geopolymers is based on the -P-O-Si-O-Al-O- bonds that take place during the hardening process.

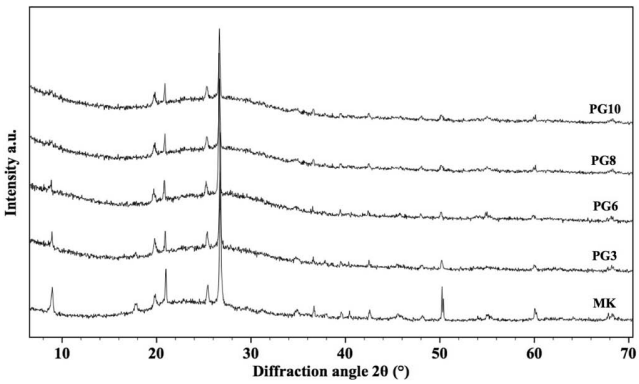

Fig. 5: XRD patterns of MK and those of the geopolymers PG3, PG6, PG8 and PG10. For peaks identification see Fig. 1.

Fig. 7 shows the concentration of different elements in the investigated samples obtained by XPS analysis. It is possible to observe opposite trends in the P and Al concentration. As expected, the amount of P in the MK sample is 0, because this element is incorporated inside the geopolymer only after the chemical reaction. However, after geopolymerization has occurred, the amount of phosphorous increases (achieving its maximum inside the PG10 sample) while the aluminium concentration decreases. As already indicated by the results of the XRD and ATR-FTIR analysis, there is a partial substitution of Si-O-Si bonds with Si-O-P bonds, which explains the trend observed during the analysis.

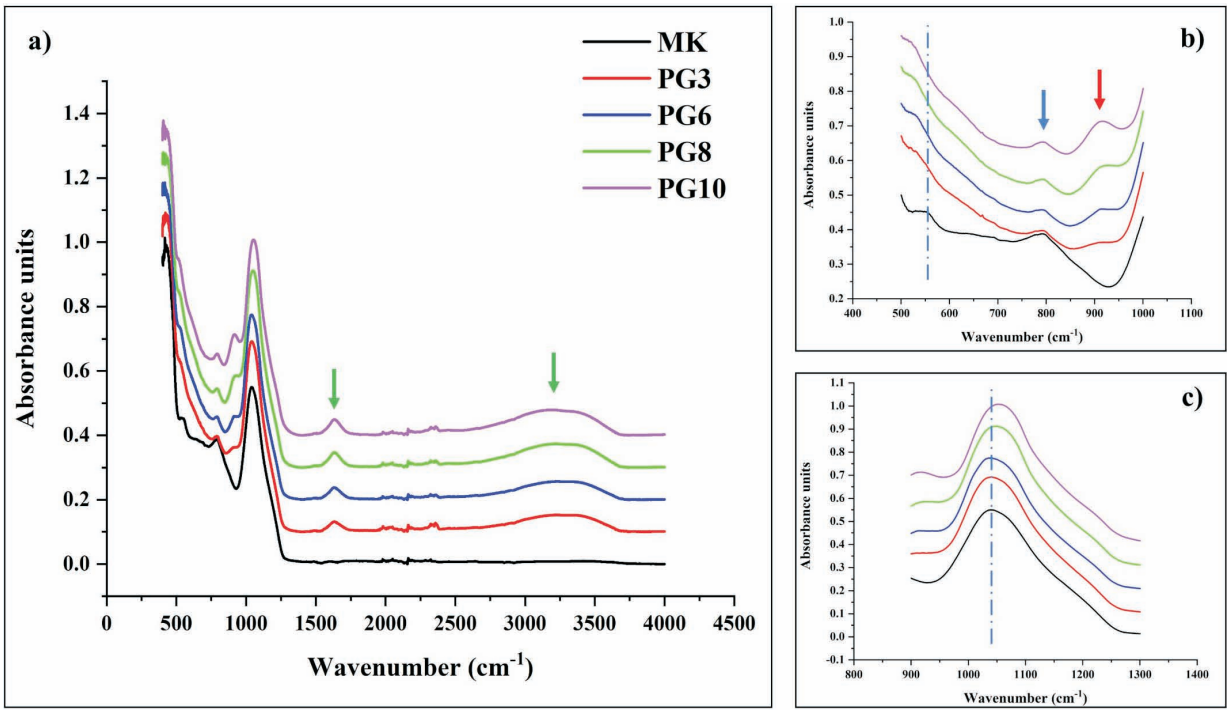

Fig. 6: ATR-FTIR spectra collected on MK and PG samples (a). Detail of two spectral windows: (b) 500 – 1 000 cm^{-1} and (c) 900 – 1 300 cm^{-1}.

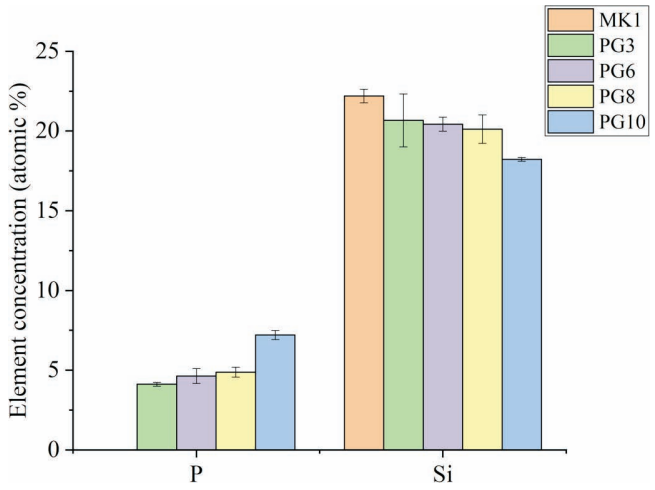

Fig. 7: Element concentration (atomic %) of P and Si in metakaolinite and geopolymer samples obtained by means of XPS.

The compressive strength data reported in Table 2 range from a minimum value of 8 MPa for composition PG1 to the maximum of 34 obtained for composition PG11. It can be observed that strength grows with decreasing slump at a constant P/Si ratio i.e. with a decreasing H_2O/total solid content, whereas it increases with increasing P/Si ratio at a constant H_2O/total solid content, as shown in Fig. 8. The above results also confirm that the strength of the geopolymers increases with an increases in the amount of phosphoric acid during their production, in agreement with the works of other researchers [42].

However, a similar mechanical behaviour would be expected for the compositions in the same area of the diagram designed by Celerier *et al.* [34] for the consolidation time at 70 °C. In fact, samples with composition PG3 and PG8 display strength values close to PG6 and PG10, respectively. The water absorption measurements highlight a complementary behaviour (see Fig. 8): as expected, materials with low strength display high water absorption, conversely high strength may be coupled with low water absorption.

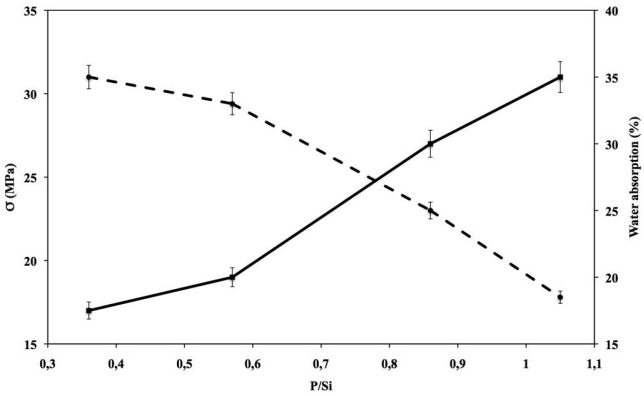

Fig. 8: Compressive strength (plain line) and water absorption (dashed line) versus P/Si at the H_2O/total solid content ratio of 0.47. Error bars are also displayed.

Table 3 shows the textural characteristics of geopolymers prepared in the present research. It can be observed that the specific surface area ranges from 39 m^2/g measured on sample PG10 to 83 for sample PG7; pore volume ranges between 0.04 and 0.05 cm^3/g whereas average pore width ranges from a minimum of 5.1 nm measured on sample PG7 to 6.8 observed on specimen PG2. Readers may think that pore volume and average pore width appear to be independent of the materials' composition, there being very little differences between the values shown in Table 3; in contrast, the specific surface area seems to be affected by materials' composition, even if a clear trend is not visible as function of the P/Si ratio, nor of the H_2O/total solid content. However similar features between materials that

exhibit the same consolidation time have already been observed [34]. In fact, Figs. 9a and 9b show the trend of dV/dlog D (cm^3/g) versus pore diameter of samples PG3 – PG6 and PG8 – PG10, respectively. Such compositions correspond to geopolymers with the same H_2O/total solid content (0.47), but different P/Si ratio: PG3 and PG6 refer to materials that require a consolidation time longer than 3 hours, PG8 and PG10 consolidate in a shorter time. Fig. 9a shows that compositions PG3 and PG6 have similar pore size distribution with a diameter between 33 and 47 Å. Composition PG3 shows a major amount of pores with large size, which, however, is not coupled with a higher average pore width (Table 3). On the other hand, materials with compositions PG8 and PG10 show a larger pore size distribution compared to that of PG3 and PG6, the pore size in these compositions ranging between 25 and 47 Å.

Figs. 10 (a-d) show the characteristics of samples PG3 (a), PG6 (b), PG8 (c) and PG10 (d) after controlled geopolymerization. It can be observed that, with increasing P/Si ratio, the porosity (coarse and fine) is progressively reduced in its dimensions and quantity; at the same time, the microstructure appears to be refined: grain size is reduced and much more uniform, thus confirming the previously discussed results.

Several authors [2–3, 8] have shown that the Si/Al ratio strongly affects the morphology of alkali-activated geopolymers as well as their structural and/or functional properties. In parallel, the literature reports that the P/Si or P/Al ratios affect the structural features as well as the mechanical performances of phosphoric-acid-based geopolymers. Going into more detail, Gao *et al.* [30] demonstrated that optimal compressive strength can be obtained in geopolymers with $H_3PO_4/Al_2O_3 = 1.3:1$; higher or lower values lead to the production of materials with lower strength. Louati *et al.* [29] showed that optimal compressive strength is developed in material having a Si/P ratio of 2.75, i.e. P/Si=0.36. Tchakouté *et al.* [42] demonstrated that optimal compressive strength may be obtained using H_3PO_4 10M solution (P/Si around 0.6) whereas a higher or lower H_3PO_4 concentration leads to the production of materials with lower strength. On the other hand, it is known that macroporosity influences the materials' mechanical behaviour more than micro- or nanoporosity. In the case of geopolymeric materials, macroporosity strongly depends on the amount of excess water that must be added to optimize mixing and workability. This excess water does not react during the geopolymerization process, remaining outside the network, and therefore escapes during drying, indicating more pores in geopolymer cements. Water absorption data measured in the geopolymers prepared in the present research range from a minimum of 17 to a maximum of 40 %, thus appearing relatively high and suggesting the presence of a large amount of macroporosity in all the compositions. It is therefore the opinion of the authors of the present paper that the effect of the excess water used to mix the geopolymeric pastes on the compressive strength of the hardened materials is more significant than that of the materials' textural characteristics. However, the present work demonstrates that an increase of the P/Si ratio enables minimization of the excess water during geopolymeric paste preparation, leading to an improvement of their compressive strength.

Table 3: Specific surface area (m^2/g), pore volume (cm^3/g) and average pore width (nm) of the geopolymers prepared.

Sample name	Specific surface area	Pore volume	Average pore width
PG1	55	0.04	6.3
PG2	54	0.05	6.8
PG3	57	0.05	6.5
PG4	56	0.05	6.6
PG5	58	0.04	6.5
PG6	61	0.04	6.2
PG7	83	0.05	5.1
PG8	79	0.05	5.1
PG9	79	0.04	5.2
PG10	39	0.05	5.9
PG11	45	0.04	5.7

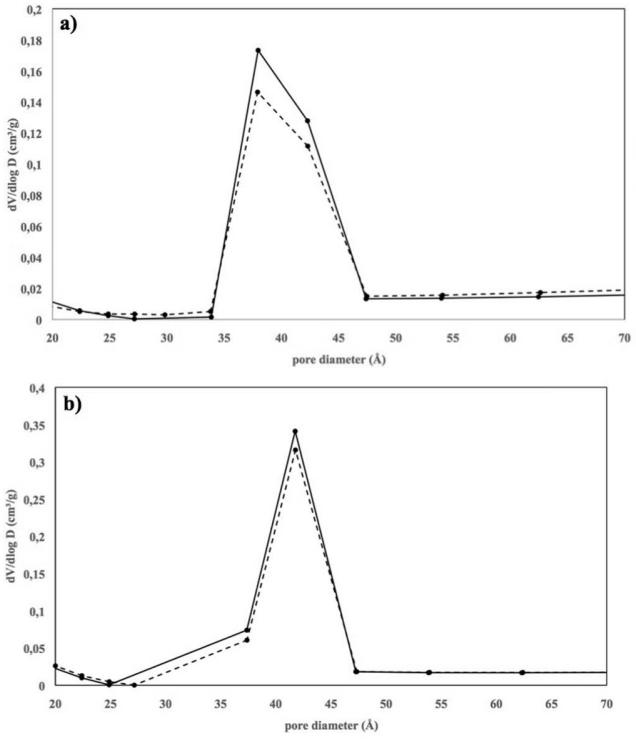

Fig. 9: Pore size distribution of geopolymers samples evaluated from N2 desorption isotherm: (a) PG3 (dashed line) and PG6 (plain line); (b) PG8 (dashed line) and PG10 (plain line).

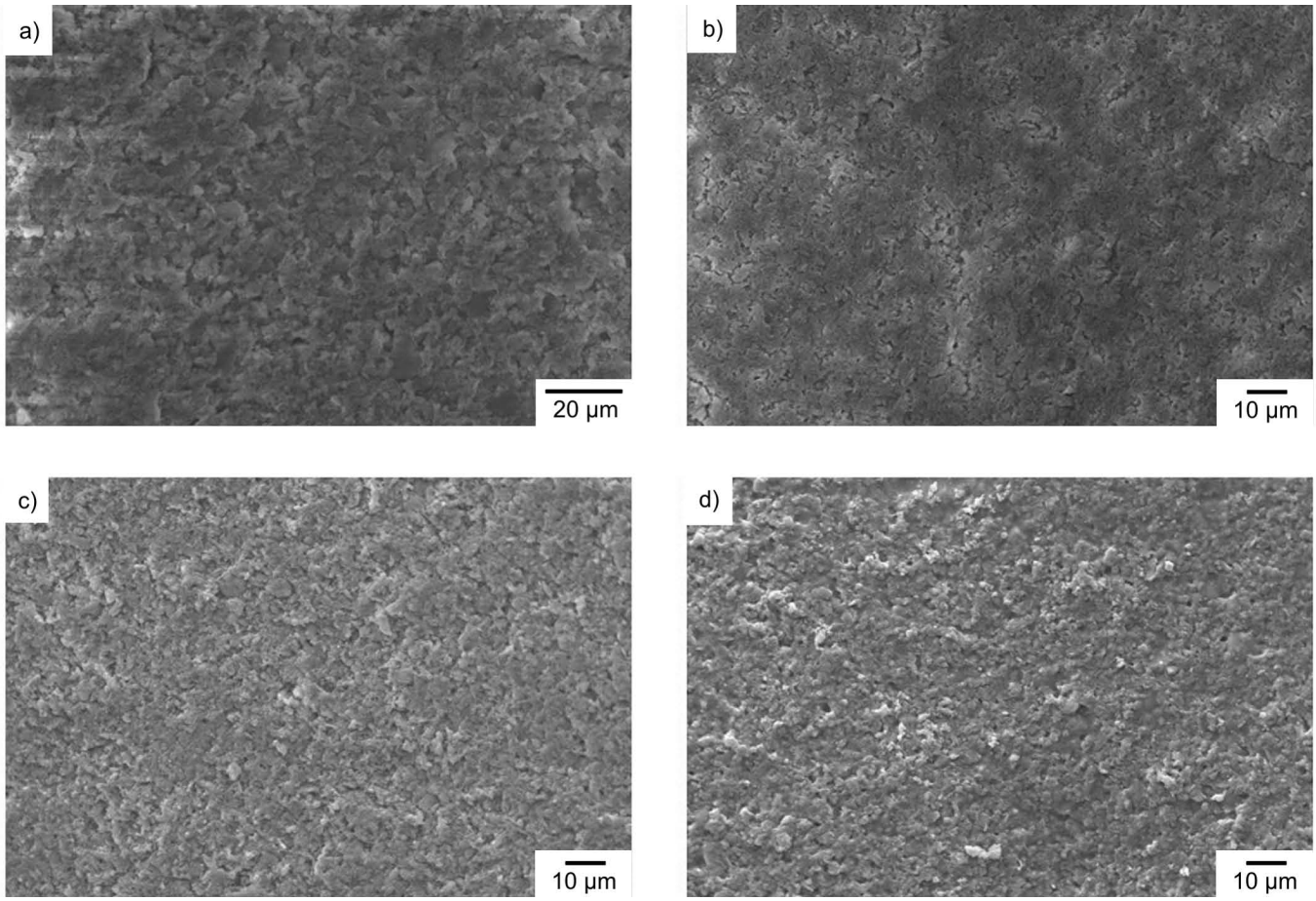

Fig. 10 a, b, c, d: SEM micrographies (1 600x) of the free surface of samples PG3 (a), PG6 (b), PG8 (c) and PG10 (d) after consolidation.

The test used to investigate the elution/stability of geopolymers in water is a modified version of the EN 12457 test, which is typically used to evaluate the release of heavy metals from contaminated products. No elution of acid was observed from the geopolymer specimens since all the solutions extracted after dipping of the geopolymers specimens in water revealed a pH ranging from 7.2 to 7.5 independent of their composition. In the parallel experiment, the weight difference of the coarse material particles submitted to the stability test, before and after the treatment, ranges from 0.2 to 0.5 %, thus suggesting good stability in water.

IV. Conclusions

Geopolymers with different compositions were prepared by mixing metakaolin, water and phosphoric acid solution in different proportions in order to obtain P/Si ratios of 0.36, 0.57. 0.86 and 1.05. The resulting pastes were cast into proper moulds and hardening was performed by aging at 10 °C for 48 h followed by thermal treatment at 40 °C for ten days.

It has been observed that:

- the workability of the geopolymeric paste improves with increasing P/Si ratio, thus enabling a reduction of the amount of water;
- XRD diffraction analysis demonstrated that quartz and anatase are almost inert versus the phosphoric acid attack whereas muscovite reacts slightly during geopolymerization. A change of the amorphous structure in all geopolymers has also been observed, this change appearing to be independent of the P/Si ratio of the composition;
- the ATR-FTIR investigation suggests that Si-O-Si bonds are partially substituted by Si-O-P and Si-O-Al bonds as a consequence of the geopolymeric reaction, the same results were obtained with XPS investigations;
- the compressive strength of the hardened materials increases with increasing P/Si ratio at a constant H_2O/total solid content, whereas their strength is lowered with increasing H_2O/total solid content at constant P/Si ratio;
- pore volume and average pore width are independent of the materials' composition; however, the specific surface area is affected by the materials' composition, even if a clear trend could not be observed as a function of the P/Si ratio, nor of the H_2O/total solid content.

References

1 Davidovits, J.: Geopolymers – inorganic polymeric new materials, *J. Therm. Anal.*, **37** [8], 1633 – 1656, (1991).

2 Hajimohammadi, A., Provis, J.L., Van Deventer, J.S.J.: Effect of alumina release rate on the mechanism of geopolymer gel formation, *Chem. Mater.*, **22** [18], 5199 – 5208, (2010).

3 Van Riessen, A., Rickard, W.D.A., Williams, R.P., van Riessen, G.A.: Methods for geopolymer formulation development

and microstructural analysis, *J. Ceram. Sci. Technol.*, **8** [3], 421 – 432, (2017).

4 Xu, H., van Deventer, J.S.J.: The geopolymerization of alumino-silicate minerals, *J. Miner. Process*, **59**, 247 – 266, (2000).

5 Khale, D., Chaudhary, R.: Mechanism of geopolymerization and factors influencing its development: A review, *J. Mater. Sci.,* **42**, 729 – 746, (2007).

6 Kamseu, E., Leonelli, C., Melo Chinje, U., Perera, D.S., Lemougna, P.N.: Polysialate matrixes from Al-rich and Si-rich metakaolins: polycondensation and physico-chemical properties, *Interceram.*, **60**, 25 – 31, (2011).

7 Carabba, L., Manzi, S., Rambaldi, E., Ridolfi, G., Bignozzi, M.C.: High-temperature behaviour of alkali-activated composites based on fly ash and recycled refractory particles, *J. Ceram. Sci. Technol.*, **8** [3], 377 – 388, (2017).

8 Constâncio Trindade, A.C., Alcamand, H.A., Ribeiro Borges, P.H., de Andrade Silva, F.: Influence of elevated temperatures on the mechanical behavior of jute-textile-reinforced geopolymers, *J. Ceram. Sci. Technol.*, **8** [3], 389 – 398, (2017).

9 Wagh, A.S.: Chemically bonded phosphate ceramics – a novel class of geopolymers, *Ceram. Trans.,* **165**, 107 – 116, (2005).

10 Cao, D., Su, D., Lu, B., Yang, Y.: Synthesis and structure characterization of geopolymeric material based on metakaolinite and phosphoric acid, *J. Chin. Ceram. Soc.*, **33**, 1385 – 1389, (2005).

11 Cu, X., Ping, L., He, Y., Chen, J., Zhou, J.: A novel aluminosilicate geopolymer material with low dielectric loss, *Mater. Chem. Phys.*, **130**, 1 – 4, (2011).

12 Le-ping, L., Xue-min, C., Shu-heng, Q., Jun-li, Y., Lin, Z.: Preparation of phosphoric acid-based porous geopolymers, *Appl. Clay Sci.*, **50**, 600 – 603, (2010).

13 Lassinantti Gualtieri, M., Romagnoli, M., Gualtieri, F.A.: Preparation of phosphoric acid-based geopolymer foams using limestone as pore forming agent – thermal properties by *in situ* XRPD and rietveld refinements, *J. Eur. Ceram. Soc.*, **35**, 3167 – 3178, (2015).

14 Krizan, D., Zivanovic, B.: Effects of dosage and modulus of water glass on early hydration of alkali-slag cements, *Cement Concrete Res.*, **32** [8], 1181 – 1188, (2002).

15 Duxson, P., Provis, J.L., Lukey, G.C., van Deventer, J.S.J.: The role of inorganic polymer technology in the development of 'green concrete', *Cement Concrete Res.*, **37** [12], 1590 – 1597, (2007).

16 Palomo, A., Grutzeck, M.W., Blanco, M.T.: Alkali-activated fly ashes: A cement for the future, *Cement Concrete Res.*, **29** [8], 1323 – 1329, (1999).

17 Sakulich, A.R., Anderson, E., Schauer, C., Barsoum, M.W.: Mechanical and microstructural characterization of an alkali-activated slag/limestone fine aggregate concrete, *Constr. Build. Mater.*, **23** [8], 2951 – 295, (2009).

18 Palomo, A., Palacios, M.: Alkali-activated cementitious materials: alternative matrices for the immobilisation of hazardous wastes - part II. stabilisation of chromium and lead, *Cement Concrete Res.*, **33,** [2], 289 – 295, (2003).

19 Leonelli, C., Kamseu, E, Lancellotti, I., Barbieri, L.: Geopolymerization as cold-consolidation techniques for hazardous and non-hazardous wastes, *Key Eng. Mater.*, **751** KEM, 527 – 531, (2017).

20 Zhang, J., Provis, J.L., Feng, D., van Deventer, J.S.J.: Geopolymers for immobilization of Cr^{6+}, Cd^{2+}, and Pb^{2+}, *J. Hazard. Mater.*, **157**, $^{2-3}$, 587 – 598, (2008).

21 Qian, G., Sun, D.D., Tay, J.H.: Immobilization of mercury and zinc in an alkali-activated slag matrix, *J. Hazard. Mater.*, **101** [1], 65 – 77, (2003).

22 Puertas, F., Fernández-Jiménez, A.: Mineralogical and microstructural characterisation of alkali-activated fly ash/slag pastes, *Cement Concrete Comp.*, **25** [3], 287 – 292, (2003).

23 Ke, X., Bernal, S.A., Ye, N., Provis, J.L., Yang, J.: One-part geopolymers based on thermally treated red Mud/NaOH blends, *J. Am. Ceram. Soc.*, **98** [1], 5 – 11, (2015).

24 Ye, N., Yang, J., Liang, S., Hu, Y., Hu, J., Xiao, B., Huang, Q.: Synthesis and strength optimization of one-part geopolymer based on red mud, *Constr. Build. Mater.*, **111**, 317 – 325, (2016).

25 Furlani, E., Maschio, S., Magnan, M., Aneggi, E., Andreatta, F., Lekka, M., Lanzutti, A., Fedrizzi, L.: Synthesis and characterization of geopolymers containing blends of unprocessed steel slag and metakaolin: The role of slag particle size, *Ceram. Int.*, **44**, 5226 – 5232, (2018).

26 Furlani, E., Magnan, M., Mingone, E., Deison, M., Aneggi, E., Andreatta, F., Fedrizzi, L., Maschio, S.: Waste olivine and silica sands boost geopolymers' performances: Experimental investigation, *Int. J. Environ. Stud.,* **76** [3], 491 – 506, (2019).

27 Liu, L.P., Cui, X.M., He, Y., Liu, S.D., Gong, S.Y.: The phase evolution of phosphoric acid-based geopolymers at elevated temperatures, *Mater. Lett.,* ***66***, 10 – 12, (2012).

28 Morsy, M.S., Rashad, A.M., Shoukry, H., Mokhtar, M.M.: Potential use of limestone in metakaolin-based geopolymer activated with H_3PO_4 for thermal insulation, *Constr. Build. Mater.,* ***22***, 117088, (2019).

29 Louati, S., Baklouti, S., Samet, B.: Geopolymers based on phosphoric acid and illito-kaolinitic clay, *Adv. Mater. Sci. Eng.*, Article ID 2359759, 7 pages, (2016).

30 Gao, L., Zheng, Y., Tang, Y., Yu, J., Yu, X., Liu, B.: Effect of phosphoric acid content on the microstructure and compressive strength of phosphoric acid-based metakaolin geopolymers, *Heliyon,* **6** [4], e03853 (2020).

31 Douiri, H., Louati, S., Baklouti, S., Arous, M., Fakhfakh, Z.: Structural, thermal and dielectric properties of phosphoric acid-based geopolymers with different amounts of H_3PO_4, *Mater. Lett.*, **116**, 9 – 12, (2014).

32 Douiri, H., Louati, S., Baklouti, S., Arous, M., Fakhfakh, Z.: Enhanced dielectric performance of metakaolin-H_3PO_4 geopolymers, *Mater. Lett.*, **164**, 299 – 302, (2016).

33 Sellami, M., Barre, M., Toumi, M.: Synthesis, thermal properties and electrical conductivity of phosphoric acid-based geopolymer with metakaolin, *Appl. Clay Sci.*, **180**, 105192, (2019).

34 Celerier, H., Jouin, J., Mathivet, V., Tessier-Doyen, N., Rossignol, S.: Composition and properties of phosphoric acid-based geopolymers, *J. Non-Crystalline Solids*, *493*, 94 – 98, (2018).

35 Gharzouni, A., Sobrados, I., Joussein, E., Baklouti, S., Rossignol, S.: Predictive tools to control the structure and the properties of metakaolin based geopolymer materials, *Colloid. Surface A,* **511**, 212 – 221, (2016).

36 Kuenzel, C., Neville, T.P., Donatello, S., Vandeperre, L., Boccaccini, A.R., Cheeseman, C.R.: Influence of metakaolin characteristics on the mechanical properties of geopolymers, *Appl. Clay Sci.*, **83 – 84**, 308 – 314, (2013).

37 Jenkins, R., Snyder, R.: Introduction to X-ray powder diffractometry, Wiley, New York, 1996.

38 Wang, Q., Li, L., Wu, C.P., Sui, Z.T.: Research on adaptability of slag-based geopolymer with superplasticizer, *Key Eng. Mater.*, **405**, 129 – 134, (2009).

39 Nematollahi, B., Sanjayan, J.: Effect of different superplasticizers and activator combinations on workability and strength of fly ash based geopolymer, *Mater. Design*, **57**, 667 – 672, (2014).

40 Cassidy, J.E.: Phosphate bonding then and now, *Am. Ceram. Soc. Bull.*, **56** [7], 640 – 643, (1977).

41 Kalyoncu, R.S.: Chemically bonded refractories – a review of the state of the art, Bureau of mines information circular, Washington D.C., 1982.

42 Tchakouté, H.K., Rüscher, C.H., Kamseu, E., Andreola, F., Leonelli, C.: Influence of the molar concentration of phosphoric acid solution on the properties of metakaolin-phosphate-

based geopolymer cements, *Appl. Clay Sci.*, **147**, 184 – 194, (2017).

[43] Tchakouté, H.K., Rüscher, C.H.: Mechanical and microstructural properties of metakaolin-based geopolymer cements from sodium waterglass and phosphoric acid solution as hardeners: A comparative study, *Appl. Clay Sci.,* **140**, 81 – 87, (2017).

[44] Louati, S., Hajjaji, W., Baklouti, S., Samet, B.: Structure and properties of new eco-material obtained by phosphoric acid attack of natural tunisian clay, *Appl. Clay Sci.*, **101**, 60 – 67, (2014).

[45] Rovnaník, P.: Effect of curing temperature on the development of hard structure of metakaolin-based geopolymer, *Constr. Build. Mater.*, **24** [7], 1176 – 1183, (2010).

[46] Criado, M., Fernández-Jiménez, A., Palomo, A.: Alkali activation of fly ash: effect of the SiO_2/Na_2O ratio. part I: FTIR study, *Microporous Mesoporous Mater.*, **106** [1 – 3], 180 – 191, (2007).

[47] Xu, T., Chen, J.Z., Han, W., Li, Z., Yu, G.: Geopolymer-organic polymer composite synthesized by the interactions of H_3PO_4 with metakaolinite powders and polyvinyl alcohol, *Part. Sci. Technol.*, **28** [6], 539 – 546, (2010).

[48] Cao, D., Su, D., Song, G.: Geopolymeric behavior and structure of lower modulus sodium silicate solutions, *J. Chinese Ceram. Soc.*, **32** [8], 1036 – 1039, (2004).